Nonlinear Observer with Time-Varying Gains for Inertial Navigation Aided by Satellite Reference Systems in Dynamic Positioning

Torleiv Håland Bryne, Thor I. Fossen and Tor A. Johansen

Abstract— The measurement quality of Global Navigation Satellites Systems (GNSS) during marine operations will vary over time. Inherently, GNSS quality changes should be handled when GNSS is utilized as aid in inertial navigation systems. In this paper we present an observer for estimating position, velocity and attitude with time-varying gains for high-performance sensor fusion based on GNSS quality and other quality indicators. The origin of the error dynamics is proven to be uniformly semiglobal exponentially stable. The concept is illustrated by simulating a vessel operating in dynamic positioning with GNSS and inertial sensors.

I. INTRODUCTION

A strapdown inertial navigation system (INS) is mounted on a navigating object or vehicle and therefore moves together with the respective body in question. The estimated position, velocity and attitude (PVA) provided by the strapdown INS is based on double and single integration of accelerometer and gyroscope measurements, respectively.

Standalone INS estimates can be accurate over shorter time horizons, however inertial sensor errors such as biases, scale factors and alignment errors propagate through integration and leads to degraded performance over time. As a consequence, INS is aided by other sensors or position reference systems to combat the long term drift of the PVA estimates.

Integration of INS and GNSS is far from novel. Maybeck [1] presents aided navigation by utilizing the extended Kalman filter (EKF). GNSS aided navigation is the primary focus of Farrell [2]. A disadvantage of the EKF is the lack of global stability guarantees due to linearization about the given trajectory. Nonlinear observer theory offers a way around these potential limitations and is applied in this paper.

In the last two decades several nonlinear observers for attitude estimation have been presented. The basis for these observers has either been a direct attitude measurement or resolving the attitude with vector measurements. The latter concept is based on comparison of vector measurements with their respective reference vectors in a given reference frame. The first principle was utilized in [3]–[5], whereas Mahony

et al. [6], Hua [7], Batista et al. [8]–[9] and Grip et al. [10] utilized vector measurements to estimate the attitude.

Integration of strapdown INS and GNSS with nonlinear observer theory was first demonstrated by Vik and Fossen [5]. The work of Vik and Fossen is based on the assumption that the attitude could be resolved independently from other measurements. A direct attitude measurement was not needed in Hua [7] and Roberts and Tayebi [11] where the INS/GNSS integration was carried out with linear GNSS velocity measurements together with inertial and magnetometer measurements. More recently, Grip et al. [12] estimated position, velocity and attitude by utilizing a rotation matrix as attitude representation with the framework of interconnected observers from [13]. The origin of the INS/GNSS integration error dynamics was proven to be global exponential stable. A semiglobal result was presented in Grip et al. [14] where the unit quaternion was utilized as attitude representation. The work of [12] and [14] included gyro bias estimation and feedback from estimated linear acceleration in inertial coordinates.

The results in Grip et al. [14] are valid with fixed observer gains related to the estimation of translational motion. The gains related to the attitude and gyro bias estimation can be time-varying as long they are sufficiently large. When GNSS quality changes should the observer gains be modified. GNSS quality can e.g. be affected by changes in satellite constellation or satellite shadow when approaching an offshore installation. Such quality changes can occur during dynamic positioning (DP) of ships and marine vessels. A DP vessel is defined in Fossen [15, Ch. 12.2.10] as: "A free-floating vessel which maintains its position (fixed location or predetermined track) exclusively by means of thrusters".

A. Contribution of Paper

This paper expands the work of Grip et al. [14] with a modified problem formulation and sensor configuration; customizing the observer for surface vessels in order to obtain high performance and robust sensor fusion. The two main contribution of this paper can be summarized as:

- In general, the GNSS height measurement has low precision. For operations at the (known) sea surface level, this measurement is replaced with a virtual measurement of the integrated height, i.e. $p_z'^n = \int_0^t p_z^n \mathrm{d}t$, to achieve increased performance related to estimation of heave and vertical acceleration in the North, East, Down reference frame.

- Expanding the work of [14], related to the estimation of translation motion, by introducing time-varying gains. In marine applications such as DP are time-varying gains beneficial when GNSS quality changes. This can e.g. prevent unnecessary measurement noise to propagate from the estimates to the control system when GNSS quality is reduced. Such gain strategy has the potential to reduce fuel cost, emissions from engines and wear of mechanical equipment such as thrusters.

B. Notation and Preliminaries

The transpose of a matrix M and vector v is denoted M^{T} and v^{T}, respectively. The identity matrix is denoted, $I_{n \times n}$ where n is the dimension. A block diagonal matrix is defined as $M := \mathrm{blkdiag}\{M_1, ..., M_n\}$ for some square matrices M_1 to M_n. Moreover, the Euclidean and Frobenius norms are denoted $\| \cdot \|$.

The unit quaternion is defined as $q := [s, \, r^{\mathsf{T}}]^{\mathsf{T}}$ where the $s \in \mathbb{R}$ denotes the real part whereas, $r \in \mathbb{R}^3$ constitutes the vector part and is given as $r = [r_1, \, r_2, \, r_3]^{\mathsf{T}}$. The conjugate of q is denoted q^* and is given as $q = [s, \, -r^{\mathsf{T}}]^{\mathsf{T}}$. Moreover, $\|q\| = 1$ from the unity constraint. The quaternion product is denoted $q = q_1 \otimes q_2$, for two unit quaternions q_1 and q_2, respectively.

The rotation matrix is denoted $R \in SO(3)$ and can be calculated according to $R(q_b^n) = I_{3 \times 3} + 2sS(r) + 2S(r)^2$, as in e.g. [14], where $S(\cdot)$ denotes the skew-symmetric matrix and is given such that $v_1 \times v_2 = S(v_1)v_2$ for two given vectors $v_1, v_2 \in \mathbb{R}^3$.

This paper employs two reference frames. The North, East, Down (NED) and the BODY frame, denoted n and b, respectively. The BODY frame is fixed to the vessel. For marine surface vessels, employing local navigation, NED is assumed to be nonrotating and fixed to the average sea surface level.

II. PROBLEM FORMULATION

We state the problem formulation for local navigation by considering

$$\dot{p}^n = v^n \tag{1}$$
$$\dot{v}^n = f^n + g^n \tag{2}$$
$$\dot{q}_b^n = T_q(q)\omega_{b/n}^b \tag{3}$$
$$\dot{b}_g^b = 0. \tag{4}$$

where p^n, v^n and f^n denote the position, velocity and specific force in NED, respectively. Moreover, an additional state of integrated vertical position, i.e. $p_z'^n = \int_0^t p_z^n \, \mathrm{d}t$ or

$$\dot{p}_z'^n = p_z^n \tag{5}$$

is introduced. q_b^n is the unit quaternion between BODY and NED. $\omega_{b/n}^b$ is the angular velocity of BODY with respect to NED expressed in BODY. The three gyro biases are denoted, b_g^b. Finally, $T(q_b^n)$ is defined as:

$$T(q_b^n) := \frac{1}{2} \begin{bmatrix} -r_1 & -r_2 & -r_3 \\ s & -r_3 & r_2 \\ r_3 & s & -r_1 \\ -r_2 & r_1 & s \end{bmatrix}, \tag{6}$$
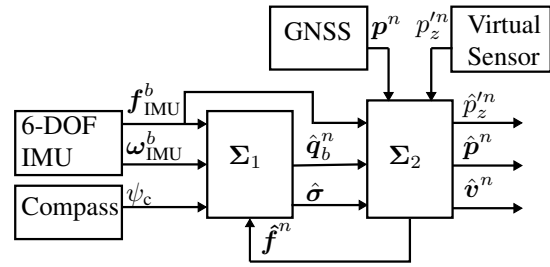

Fig. 1. Observer Structure. The attitude and observer translational motion observer is denoted Σ_1 and Σ_2, respectively. Σ_1 provides an estimate of the unit quaternion, $\hat{q}$, together with an estimate on the gyro biases, $\hat{b}^b$. The latter is estimated to improve the estimate of $\hat{q}$. The signals $\hat{q}_b^n$ and $\hat{\sigma}$ are utilized by Σ_2 to estimate the specific force, $\hat{f}^n$, in NED as seen in (9d)–(9e). Moreover, $\hat{f}^n$ is fed back to Σ_1 and is utilized as a reference vector in the attitude estimation.

for $q_b^n = [s, \, r^{\mathsf{T}}]^{\mathsf{T}}$. The system (1)–(4) is based on the formulation in [14] with the difference that NED is the navigation frame and the gravity vector, g^n, is known. This is valid in DP since the operation is confined to a small geographical area. Then, the gravity error components will be significantly less than the GNSS standard deviation. The total feedback interconnected observer is illustrated in Fig. 1 and described in Section III-A and III-B.

A. Sensor Configuration

The results in this paper are based upon the following sensor configuration of IMU, GNSS, compass and virtual measurements:

1) Horizontal position measurement from GNSS given in NED: $p_{\mathrm{gnss},xy}^n = \mathrm{diag}\{p_x^n, p_y^n\}$
2) Virtual measurement: $p_z'^n = 0$, for all $t \geq 0$, motivated by Godhavn [16]. The mean vertical position of the vessel is assumed zero over time since the wave-induced motion in heave oscillates about the sea surface. Hence, from Godhavn [16], the following can be stated: $\lim_{T \to \infty} \frac{1}{T} \int_0^T p_z^n(t)\mathrm{d}t = 0$.
3) Angular velocity measurement in BODY from a three axis rate gyro with biases: $\omega_{\mathrm{IMU}}^b = \omega_{b/n}^b + b_g^b$. The biases, b_g^b, in (4) are constant.
4) Acceleration measurements providing specific force in BODY: $f_{\mathrm{IMU}}^b = f^b$. Accelerometer biases are assumed to be compensated at system start up or by online estimation, utilizing e.g. Grip et al. [10, Sec. VI], if the acceleration is persistently exciting.
5) Heading measurement from a compass: $\psi_c = \psi$.

B. Assumptions

As in [14], the bounds of the specific force and the gyro biases are denoted, M_f and M_b. Also here is the angular velocity, $\omega_{b/n}^b$, and the time derivative of the specific force, $\dot{f}^b$, assumed to be uniformly bounded. Moreover, there exist a constant $c_{\mathrm{obs}} > 0$ such that for all $t \geq 0$, $\|c^b \times f^b\| \geq c_{\mathrm{obs}}, \forall t \geq 0$, yielding uniform observability.

III. NONLINEAR OBSERVER DESIGN

As seen in Fig. 1, the nonlinear observer for estimating PVA is constructed in two steps. The first stage is to estimate

the attitude, represented by the unit quaternion q_b^n. The three gyro biases, b_g^b, are also estimated. The second stage is to estimate the velocity and the position in NED by exploiting the attitude estimate, $\hat{q}$, and the injection term of the attitude observer, $\hat{\sigma}$.

The overall stability of the interconnected observer with fixed gains was proven to be uniformly semiglobal exponentially stable (USGES) by Grip et al. [14]. We will change one of the attitude vector measurements before augmenting the translation motion state space and expanding the translational motion observer to handle time-varying gains.

A. Attitude Observer with Compass Vector Measurement

The attitude observer Σ_1, similar to Grip et al. [14], is given as

$$\Sigma_1 = \begin{cases} \dot{\hat{q}}_b^n = T(\hat{q}_b^n)(\omega_{b/n,\text{IMU}}^b - \hat{b}_g^b + \hat{\sigma}) & (7a) \\ \dot{\hat{b}}_g^b = \text{Proj}(\hat{b}_g^b, -k_I(t)\hat{\sigma}). & (7b) \end{cases}$$

where the attitude estimate $\hat{q}$ is represented as a unit quaternion and the gyro bias estimate is denoted $\hat{b}_g^b$. However, the Earth's rotation is neglected. The injection term, with a compass vector measurement, is given by

$$\hat{\sigma} = k_1(t)f^b \times R(\hat{q})^\mathsf{T}\hat{f}^n + k_2(t)c^b \times R(\hat{q})^\mathsf{T}c^n \quad (8)$$

where $k_I(t) > 0$ in (7b) and the gains in (8) satisfies $k_1(t) \geq k_P$ and $k_2(t) \geq k_P$ for some $k_P > 0$. The vector measurement based on ψ_c, from the compass, is defined as $c^b := [\cos(\psi_c), -\sin(\psi_c), 0]^\mathsf{T}$ whereas the reference vector is defined as $c^n := [1, 0, 0]^\mathsf{T}$. f^b is measured specific force from the accelerometer. The estimate of the specific force in NED, $\hat{f}^n$, is fed back to the attitude observer from the translational motion observer, Σ_2. See Fig. 1 and Section III-B for details.

Finally, $\text{Proj}(\cdot, \cdot)$ denotes the parameter projection such that the gyro bias estimate is confined to a compact set, $\|\hat{b}_g^b\| \leq M_b$, as with the previous results presented by Grip et al. [10], [12] and [14].

B. Augmented Translation Motion Observer with Time-varying Gains

The main result of this paper is obtained by extending the work of [14] with:

1) The state space augmentation, $p_z'^n = \int_0^t p_z^n \mathrm{d}t$
2) Introduction of a time-varying observer gains by replacing the combined high-gain/regular gain, $K = K_\theta$, with $K(t) = \vartheta(t)K_\theta$ as given in (9a)–(9d).

K_θ is defined as $K_\theta := \theta L_\theta^{-1} K_0$, where L_θ is given in Appendix I. Design flexibility and performance enhancement are obtained if $\vartheta(t)$ is chosen properly.

The total augmented observer Σ_2 is given as

$$\Sigma_2 = \begin{cases} \dot{\hat{p}}_z'^n = \hat{p}_z^n + \vartheta(t)\theta K_{p_z'p_z'}\tilde{p}_z' & (9a) \\ \dot{\hat{p}}^n = \hat{v}^n + \vartheta(t)\theta^2 \begin{bmatrix} 0 & K_{pp} \\ K_{pp_z'} & \mathbf{0}_{1\times 2} \end{bmatrix} \begin{bmatrix} \tilde{p}_z' \\ \tilde{p}_{xy} \end{bmatrix} & (9b) \\ \dot{\hat{v}}^n = \hat{f}^n + g^n + \vartheta(t)\theta^3 \begin{bmatrix} 0 & K_{vp} \\ K_{vp_z'} & \mathbf{0}_{1\times 2} \end{bmatrix} \begin{bmatrix} \tilde{p}_z' \\ \tilde{p}_{xy} \end{bmatrix} & (9c) \\ \dot{\hat{\xi}} = -R(\hat{q}_b^n)S(\hat{\sigma})f_{\text{IMU}}^b \\ \quad + \vartheta(t)\theta^4 \begin{bmatrix} 0 & K_{\xi p} \\ K_{\xi p_z'} & \mathbf{0}_{1\times 2} \end{bmatrix} \begin{bmatrix} \tilde{p}_z' \\ \tilde{p}_{xy} \end{bmatrix} & (9d) \\ \hat{f}^n = R(\hat{q}_b^n)f_{\text{IMU}}^b + \xi, & (9e) \end{cases}$$

where $\tilde{p}_z' = p_z'^n - \hat{p}_z'^n$ and $\tilde{p}_{xy} = [p_x^n - \hat{p}_x^n, p_y^n - \hat{p}_y^n]^\mathsf{T}$ are the innovation signals. ξ is an intermediate state providing information of the translation motion to the specific force estimate, $\hat{f}^n$. The signals $\hat{q}_b^n$ and $\hat{\sigma}$ are provided by Σ_1.

The observer structure can be written as:

$$\dot{\hat{x}} = (A - \vartheta(t)K_\theta C)\hat{x} + B\hat{d}$$
$$= (A - \vartheta(t)\theta L_\theta^{-1} K_0 C)\hat{x} + B\hat{d} \quad (10)$$

with $\hat{x} = [p_z'^n, (\hat{p}^n)^\mathsf{T}, (\hat{v}^n)^\mathsf{T}, (\hat{f}^n)^\mathsf{T}]^\mathsf{T}$ and $\hat{d} = R(\hat{q})(S(\omega_{b/n}^b + \tilde{b}))f_{\text{IMU}}^b + \dot{f}^b)$. The unknown signals $\tilde{b}$ and $\dot{f}^b$ are the estimation error of b_g^b from Σ_1 given as $\tilde{b} = b_g^b - \hat{b}_g^b$ and the derivative of the specific force, respectively. In addition, the remaining matrices from (10) are given as:

$$A = \begin{bmatrix} 0 & 0\,0\,1 & \mathbf{0}_{1\times 3} & \mathbf{0}_{1\times 3} \\ \mathbf{0}_{3\times 1} & \mathbf{0}_{3\times 3} & I_{3\times 3} & \mathbf{0}_{3\times 3} \\ \mathbf{0}_{3\times 1} & \mathbf{0}_{3\times 3} & \mathbf{0}_{3\times 3} & I_{3\times 3} \\ \mathbf{0}_{3\times 1} & \mathbf{0}_{3\times 3} & \mathbf{0}_{3\times 3} & \mathbf{0}_{3\times 3} \end{bmatrix}, \quad B = \begin{bmatrix} \mathbf{0}_{1\times 3} \\ \mathbf{0}_{3\times 3} \\ \mathbf{0}_{3\times 3} \\ I_{3\times 3} \end{bmatrix},$$

$$C = \begin{bmatrix} 1 & 0 & 0 & \mathbf{0}_{1\times 7} \\ 0 & 1 & 0 & \mathbf{0}_{1\times 7} \\ 0 & 0 & 1 & \mathbf{0}_{1\times 7} \end{bmatrix}, \quad (11)$$

$$K_0 = \begin{bmatrix} K_{p_z'p_z'} & \mathbf{0}_{1\times 2} & K_{p_zp_z'} & \mathbf{0}_{1\times 2} & K_{v_zp_z'} & \mathbf{0}_{1\times 2} & K_{\xi_zp_z'} \\ \mathbf{0}_{2\times 1} & K_{pp} & \mathbf{0}_{2\times 1} & K_{vp} & \mathbf{0}_{2\times} & K_{\xi p} & \mathbf{0}_{2\times 1} \end{bmatrix}^\mathsf{T},$$

The nominal stationary gain K_0 can be chosen freely in order to make $A - K_0 C$ Hurwitz. $\theta \geq 1$ is a high-gain tuning parameter used to guarantee stability and robustness with respect to the uncertainties in $\hat{d}$. The time-varying scalar $\vartheta(t) \geq \tau > 0$, can e.g. be chosen by taking into account the horizontal GNSS accuracy reported by the GNSS receiver.

C. Stability Analysis

In order to state the main result of the total interconnected observer, $\Sigma_1 - \Sigma_2$, the respective estimation errors of the translational motion are defined in the following manner; $\tilde{p}_z' := p_z'^n - \hat{p}_z'^n$, $\tilde{p} := p^n - \hat{p}^n$, $\tilde{v} := v^n - \hat{v}^n$ and $\tilde{f} := f^n - \hat{f}^n$. The attitude and gyro bias estimation error are defined as $\tilde{q} := q_b^n \otimes \hat{q}_b^{n*}$ and $\tilde{b} := b_g^b - \hat{b}_g^b$, respectively.

The constraint of the unit quaternion yield zero estimation error when $\tilde{s} = 1$ or equivalently $\|\tilde{r}\| = 0$. Hence, $\tilde{s} = 0$ corresponds to the maximum attitude error of $180°$ about some axis. As in Grip et al. [14] we define a set $D_q(\epsilon) := \{\tilde{q} \,|\, |\tilde{s}| > \epsilon\}$ which represents the attitude errors bounded away from $180°$ by a margin determined by $\epsilon \in (0, \frac{1}{2})$. Furthermore, the combined estimation error of Σ_1 is defined

as $\tilde{\boldsymbol{\chi}} := [\tilde{\boldsymbol{r}}^\mathsf{T}, \tilde{\boldsymbol{b}}^\mathsf{T}]^\mathsf{T}$ similar to [14], while the combined estimation error of $\boldsymbol{\Sigma}_2$ is defined as $\tilde{\boldsymbol{x}} := [\tilde{p}_z', \tilde{\boldsymbol{p}}, \tilde{\boldsymbol{v}}, \tilde{\boldsymbol{f}}]^\mathsf{T}$. Now, the main result is stated as:

Theorem 1 (USGES of $\boldsymbol{\Sigma}_1$–$\boldsymbol{\Sigma}_2$): Let $D \subset \mathbb{R}^{10}$ be an arbitrary compact set containing the origin, and let $\bar{\epsilon} \in (0, \frac{1}{2})$ be an arbitrary constant. Furthermore, let k_P be chosen to ensure stability according to [10, Theorem 1] for $\boldsymbol{\Sigma}_1$ with known $\boldsymbol{f}^n$, with respect to some $\epsilon < \bar{\epsilon}$. Also let $\boldsymbol{P} = \boldsymbol{P}^\mathsf{T} > 0$ be the solution of the algebraic Riccati equation

$$\boldsymbol{AP} + \boldsymbol{PA}^\mathsf{T} + \boldsymbol{Q} - 2\tau \boldsymbol{PC}^\mathsf{T}\boldsymbol{CP} = 0 \qquad (12)$$

where $\boldsymbol{Q} = \boldsymbol{Q}^\mathsf{T} > 0$. Then, there exist a $\theta^* \geq 1$, a scalar $\tau > 0$ and a $\vartheta(t) \geq \tau$ such that for $\theta \geq \theta^*$, some gain $\boldsymbol{K}_0 = \boldsymbol{PC}^\mathsf{T}$ and constants $K > 0$ and $\lambda > 0$ yield

$$\sqrt{\|\tilde{\boldsymbol{x}}\|^2 + \|\tilde{\boldsymbol{\chi}}\|^2} \leq K e^{-\lambda t} \sqrt{\|\tilde{\boldsymbol{x}}(0)\|^2 + \|\tilde{\boldsymbol{\chi}}(0)\|^2},$$

for all initial condition such that $(\tilde{p}_z'(0) \times \tilde{\boldsymbol{p}}(0) \times \tilde{\boldsymbol{v}}(0) \times \tilde{\boldsymbol{\xi}}(0)) \in D$, $\tilde{\boldsymbol{q}}(0) \in D_q(\bar{\epsilon})$, and $\|\tilde{\boldsymbol{b}}_g^b(0)\| \leq M_b$. Consequently, the origin of $\boldsymbol{\Sigma}_1$–$\boldsymbol{\Sigma}_2$ is USGES.

Proof: The error dynamics of $\tilde{p}_z'$, $\tilde{\boldsymbol{p}}$ and $\tilde{\boldsymbol{v}}$ are given as

$$\dot{\tilde{p}}_z' = \tilde{p}_z - \vartheta(t)\theta K_{p_z' p_z'}\tilde{p}_z'$$

$$\dot{\tilde{\boldsymbol{p}}} = \tilde{\boldsymbol{v}} - \vartheta(t)\theta^2 \begin{bmatrix} \boldsymbol{0}_{2\times1} & \boldsymbol{K}_{pp} \\ K_{p_z p_z'} & \boldsymbol{0}_{1\times2} \end{bmatrix} \begin{bmatrix} \tilde{p}_z' \\ \tilde{\boldsymbol{p}}_{xy} \end{bmatrix}$$

$$\dot{\tilde{\boldsymbol{v}}} = \tilde{\boldsymbol{f}} + \boldsymbol{g}^n - \vartheta(t)\theta^3 \begin{bmatrix} \boldsymbol{0}_{2\times1} & \boldsymbol{K}_{vp} \\ K_{v_z p_z'} & \boldsymbol{0}_{1\times2} \end{bmatrix} \begin{bmatrix} \tilde{p}_z' \\ \tilde{\boldsymbol{p}}_{xy} \end{bmatrix}.$$

It can be shown that

$$\dot{\tilde{\boldsymbol{f}}} = \tilde{\boldsymbol{d}} - \vartheta(t)\theta^4 \begin{bmatrix} \boldsymbol{0}_{2\times1} & \boldsymbol{K}_{\xi p} \\ K_{\xi_z p_z'} & \boldsymbol{0}_{1\times2} \end{bmatrix} \begin{bmatrix} \tilde{p}_z' \\ \tilde{\boldsymbol{p}}_{xy} \end{bmatrix},$$

where $\tilde{\boldsymbol{d}} = (\boldsymbol{I}_{3\times3} - \tilde{\boldsymbol{R}}^\mathsf{T})\boldsymbol{R}(\boldsymbol{q}_b^n)\big(\boldsymbol{S}(\boldsymbol{\omega}_{b/n}^b)\boldsymbol{f}^b + \dot{\boldsymbol{f}}^b\big) - \tilde{\boldsymbol{R}}^\mathsf{T}\boldsymbol{R}(\boldsymbol{q}_b^n)\boldsymbol{S}(\tilde{\boldsymbol{b}})\boldsymbol{f}^b$ with $\tilde{\boldsymbol{R}} = \boldsymbol{R}(\boldsymbol{q}_b^n)\boldsymbol{R}(\hat{\boldsymbol{q}}_b^{n*}) = \boldsymbol{R}(\tilde{\boldsymbol{q}})$. Then, the total error dynamics becomes

$$\dot{\tilde{\boldsymbol{x}}} = (\boldsymbol{A} - \vartheta(t)\boldsymbol{K}_\theta\boldsymbol{C})\tilde{\boldsymbol{x}} + \boldsymbol{B}\tilde{\boldsymbol{d}}. \qquad (13)$$

The transformed error dynamics (Appendix I) with $\boldsymbol{\eta} := [\eta_1, \boldsymbol{\eta}_2, \boldsymbol{\eta}_3, \boldsymbol{\eta}_4]^\mathsf{T}$ where $\eta_1 := \tilde{p}_z'$, $\boldsymbol{\eta}_2 := \tilde{\boldsymbol{p}}/\theta$, $\boldsymbol{\eta}_3 := \tilde{\boldsymbol{v}}/\theta^2$ and $\boldsymbol{\eta}_4 := \tilde{\boldsymbol{f}}/\theta^3$, similar to [14], can be expressed as

$$\frac{1}{\theta}\dot{\boldsymbol{\eta}} = (\boldsymbol{A} - \boldsymbol{K}_0\boldsymbol{C})\boldsymbol{\eta} + \boldsymbol{\rho}(t, \tilde{\boldsymbol{\chi}}) \qquad (14)$$

where $\boldsymbol{\rho}(t, \tilde{\boldsymbol{\chi}}) = [0, \boldsymbol{0}_{3\times1}^\mathsf{T}, \boldsymbol{0}_{3\times1}^\mathsf{T}, \frac{1}{\theta^4}\tilde{\boldsymbol{d}}^\mathsf{T}]^\mathsf{T}$. See Appendix I for details.

The Lyapunov function candidate (LFC) is defined as $U := \frac{1}{\theta}\boldsymbol{\eta}^\mathsf{T}\boldsymbol{P}^{-1}\boldsymbol{\eta}$. Differentiation along the trajectories of (14) gives

$$\dot{U} = \frac{1}{\theta}\dot{\boldsymbol{\eta}}^\mathsf{T}\boldsymbol{P}^{-1}\boldsymbol{\eta} + \frac{1}{\theta}\boldsymbol{\eta}^\mathsf{T}\boldsymbol{P}^{-1}\dot{\boldsymbol{\eta}}$$
$$= \boldsymbol{\eta}^\mathsf{T}(\boldsymbol{P}^{-1}\boldsymbol{A} + \boldsymbol{A}^\mathsf{T}\boldsymbol{P}^{-1})\boldsymbol{\eta} - \vartheta(t)\boldsymbol{\eta}^\mathsf{T}\boldsymbol{P}^{-1}\boldsymbol{K}_0\boldsymbol{C}\boldsymbol{\eta}$$
$$- \vartheta(t)\boldsymbol{\eta}^\mathsf{T}\boldsymbol{C}^\mathsf{T}\boldsymbol{K}_0^\mathsf{T}\boldsymbol{P}^{-1}\boldsymbol{\eta} + 2\boldsymbol{\eta}^\mathsf{T}\boldsymbol{P}^{-1}\boldsymbol{\rho}(t, \tilde{\boldsymbol{\chi}}). \qquad (15)$$

By using that $\boldsymbol{K}_0 = \boldsymbol{PC}^\mathsf{T}$, resolving the transposes and exploiting that $\boldsymbol{P} = \boldsymbol{P}^\mathsf{T}$ gives

$$\dot{U} = \boldsymbol{\eta}^\mathsf{T}\boldsymbol{P}^{-1}(\boldsymbol{AP} + \boldsymbol{PA}^\mathsf{T})\boldsymbol{P}^{-1}\boldsymbol{\eta}$$
$$- 2\vartheta(t)\boldsymbol{\eta}^\mathsf{T}\boldsymbol{C}^\mathsf{T}\boldsymbol{C}\boldsymbol{\eta} + 2\boldsymbol{\eta}^\mathsf{T}\boldsymbol{P}^{-1}\boldsymbol{\rho}(t, \tilde{\boldsymbol{\chi}}). \qquad (16)$$

Furthermore, by inserting (12) into (16) gives

$$\dot{U} = -\boldsymbol{\eta}^\mathsf{T}\boldsymbol{P}^{-1}\boldsymbol{Q}\boldsymbol{P}^{-1}\boldsymbol{\eta} - 2(\vartheta(t) - \tau)\boldsymbol{\eta}^\mathsf{T}\boldsymbol{C}^\mathsf{T}\boldsymbol{C}\boldsymbol{\eta}$$
$$+ 2\boldsymbol{\eta}^\mathsf{T}\boldsymbol{P}^{-1}\boldsymbol{\rho}(t, \tilde{\boldsymbol{\chi}}). \qquad (17)$$

Then, (17) can be simplified further since $\vartheta(t) \geq \tau > 0$ yielding,

$$\dot{U} \leq -\boldsymbol{\eta}^\mathsf{T}\boldsymbol{P}^{-1}\boldsymbol{Q}\boldsymbol{P}^{-1}\boldsymbol{\eta} + 2\boldsymbol{\eta}^\mathsf{T}\boldsymbol{P}^{-1}\boldsymbol{\rho}(t, \tilde{\boldsymbol{\chi}}). \qquad (18)$$

Moreover, since $\|\boldsymbol{I}_{3\times3} - \tilde{\boldsymbol{R}}^\mathsf{T}\| = \|\tilde{s}\boldsymbol{S}(\tilde{\boldsymbol{r}}) - \boldsymbol{S}(\tilde{\boldsymbol{r}}^2)\| \leq 2\|\tilde{\boldsymbol{r}}\|$, a bound of $\boldsymbol{\rho}(t, \tilde{\boldsymbol{\chi}})$ can be given as $\|\boldsymbol{\rho}(t, \tilde{\boldsymbol{\chi}})\| \leq \frac{1}{\theta^4}\gamma_1\|\tilde{\boldsymbol{\chi}}\|$, where $\tilde{\boldsymbol{\chi}} = [\tilde{\boldsymbol{r}}^\mathsf{T}, \tilde{\boldsymbol{b}}^\mathsf{T}]^\mathsf{T}$, for some $\gamma_1 > 0$ independent of θ. Hence, $\dot{U}$ can take the following form

$$\dot{U} \leq \lambda_{\min}(\boldsymbol{Q})\lambda_{\min}(\boldsymbol{P}^{-1})^2\|\boldsymbol{\eta}\|^2 + \frac{2\|\boldsymbol{P}^{-1}\|}{\theta^4}\gamma_1\|\boldsymbol{\eta}\|\|\tilde{\boldsymbol{\chi}}\|. \qquad (19)$$

Since the reference vector $\boldsymbol{f}^n$, in (7)–(8), is not known, but estimated, we turn the attention back to the dynamics of $\tilde{s}$. The attitude observer of (7)–(8), with the injection term $\boldsymbol{\sigma}$ based on known $\boldsymbol{f}^n$ and the error dynamics,

$$\dot{\tilde{s}} = \frac{1}{2}\tilde{\boldsymbol{r}}^\mathsf{T}\boldsymbol{R}(\boldsymbol{q}_b^n)(\tilde{\boldsymbol{b}} + \boldsymbol{\sigma}) \qquad (20)$$

$$\dot{\tilde{\boldsymbol{r}}} = -\frac{1}{2}(\tilde{s}\boldsymbol{I}_{3\times3} - \boldsymbol{S}(\tilde{\boldsymbol{r}}))\boldsymbol{R}(\boldsymbol{q}_b^n)(\tilde{\boldsymbol{b}} + \boldsymbol{\sigma}) \qquad (21)$$

$$\dot{\tilde{\boldsymbol{b}}} = -\text{Proj}(\hat{\boldsymbol{b}}_g^b, -k_I\boldsymbol{\sigma}), \qquad (22)$$

was proven to be USGES in Grip et al. [10]. First, Grip et al. defines $V(\tilde{s}) := 1 - \tilde{s}^2 = \|\tilde{\boldsymbol{r}}\|^2$ and $\dot{V} = M - k_P c_{\text{obs}}^2\alpha(\tilde{s})$, where $\alpha(\tilde{s}) = \tilde{s}^2(1 - \tilde{s}^2)$. Moreover, from [10], a sufficiently large k_P and $|\tilde{s}| = \epsilon$ imply that $\dot{V} = M - k_P c_{\text{obs}}^2\alpha(\epsilon)$. This results in the trajectories not being able to escape the region defined by $|\tilde{s}| \geq \epsilon$. Furthermore, $\dot{\tilde{s}}$ can be expressed as

$$\dot{\tilde{s}} = \frac{1}{2}\tilde{\boldsymbol{r}}^\mathsf{T}\boldsymbol{R}(\boldsymbol{q}_b^n)(\tilde{\boldsymbol{b}} + \boldsymbol{\sigma}) + \mu_1, \qquad (23)$$

where $\mu_1 = \frac{1}{2}\tilde{\boldsymbol{r}}^\mathsf{T}\boldsymbol{R}(\boldsymbol{q}_b^n)(\hat{\boldsymbol{\sigma}} - \boldsymbol{\sigma})$, by taking into account (20) and that $\hat{\boldsymbol{\sigma}}$, instead of $\boldsymbol{\sigma}$, is utilized as the injection term. Moreover, μ_1 has the property $|\mu_1| \leq \frac{1}{2}k_1\|\boldsymbol{f}^b\|\|\tilde{\boldsymbol{r}}\|\|\tilde{\boldsymbol{f}}\| \leq \gamma_2\|\tilde{\boldsymbol{r}}\|\|\tilde{\boldsymbol{f}}\|$ for a $\gamma_2 > 0$ independent of θ. We also write the bound of μ_1, $|\mu_1| \leq \theta^3\gamma_2\|\tilde{\boldsymbol{r}}\|\|\boldsymbol{n}\|$. By following the steps of [14, Proof Theorem 1] we also have $|\dot{\tilde{s}}| \leq \frac{1}{2}(\|\tilde{\boldsymbol{b}}\| + \|\hat{\boldsymbol{\sigma}}\|)$. Since $\|\tilde{\boldsymbol{b}}\| \leq M$ and $\hat{\boldsymbol{\sigma}}$ only consist of bounded signals we have $|\dot{\tilde{s}}| \leq M_s$ for a $M_s > 0$ independent of θ.

Motivated by Grip et al. [14, Lemma 2], the bound of $\tilde{\boldsymbol{x}}$ can be given as $\|\tilde{\boldsymbol{x}}\| \leq \delta$, obtained for all $t \geq T$, for some δ, as presented in Lemma 1, Appendix II. Furthermore, δ can be defined as $\delta := k_P c_{\text{obs}}^2(\alpha(\epsilon + \tilde{\epsilon}/2) - \alpha(\epsilon))/(2\gamma_2) > 0$ and $T = \tilde{\epsilon}/(2M_s)$, where $\tilde{\epsilon} := \bar{\epsilon} - \epsilon$, and let θ be sufficiently large such that for all $t \geq T$, $\|\tilde{\boldsymbol{x}}\| \leq \delta$. Then, as in [14, Proof Theorem 1],

$$|\tilde{s}(T)| \geq |\tilde{s}(0)| - \int_0^T |\dot{\tilde{s}}(t)|\,\mathrm{d}t \leq \bar{\epsilon} - M_s\tilde{\epsilon}/(2M_s) = \epsilon + \tilde{\epsilon}/2,$$

and for all $t \geq T$, $|\mu_1| \leq \gamma_2\|\tilde{\boldsymbol{r}}\|\|\boldsymbol{\eta}\| \leq \gamma_2\delta \leq k_P c_{\text{obs}}^2(\alpha(\epsilon + \tilde{\epsilon}/2) - \alpha(\epsilon))/2$. Now, it follows for $t \geq T$ that the derivative of $V(\tilde{s})$ yields

$$\dot{V} \leq M - k_P c_{\text{obs}}^2\alpha(\tilde{s}) + 2|\tilde{s}\mu_1|$$
$$\leq M - k_P c_{\text{obs}}^2(\alpha(\tilde{s}) - \alpha(\epsilon + \tilde{\epsilon}/2) + \alpha(\epsilon)).$$

Then, with the reference to the proof of [10, Theorem 1] it follows for $|\tilde{s}| = \epsilon + \tilde{\epsilon}/2$ that $\dot{V} \leq M - k_P\, c_{\text{obs}}^2 \alpha(\epsilon) < 0$. Hence, $\tilde{q}$ cannot escape the set $D_q(\epsilon + \tilde{\epsilon}/2) \subset D_q(\epsilon)$ and we can assume $|\tilde{s}| \geq \epsilon$ in the remainder of the analysis.

By taking in account (21)–(22) and that $\hat{\sigma}$ is the injection term, the error dynamics of $\tilde{r}$ and $\tilde{b}$ are written

$$\dot{\tilde{r}} = -\frac{1}{2}\left(\tilde{s}\boldsymbol{I}_{3\times 3} - \boldsymbol{S}(\tilde{r})\right)\boldsymbol{R}(\boldsymbol{q}_b^n)(\tilde{b} + \boldsymbol{\sigma}) + \boldsymbol{\mu}_2 \quad (24)$$

$$\dot{\tilde{b}} = -\text{Proj}(\hat{b}_g^b, -k_I\boldsymbol{\sigma}) + \boldsymbol{\mu}_3. \quad (25)$$

Hence, $\boldsymbol{\mu}_2$ and $\boldsymbol{\mu}_3$ take the form, $\boldsymbol{\mu}_2 = \frac{1}{2}(\tilde{s}\boldsymbol{I}_{3\times 3} - \boldsymbol{S}(\tilde{r}))\boldsymbol{R}(\boldsymbol{q}_b^n)(\boldsymbol{\sigma} - \hat{\boldsymbol{\sigma}})$ and $\boldsymbol{\mu}_3 = -\text{Proj}(\hat{b}_g^b, -k_I\boldsymbol{\sigma}) - \text{Proj}(\hat{b}_g^b, -k_I\hat{\boldsymbol{\sigma}})$. Then, $\|\boldsymbol{\mu}_2\| \leq \gamma_3\|\tilde{f}\| \leq \theta^3\gamma_3\|\boldsymbol{\eta}\|$ for some $\gamma_3 > 0$ independent of θ. From the properties of the parameter projection, it can be shown that $\|\boldsymbol{\mu}_3\| \leq \gamma_4\|\tilde{f}\| \leq \theta^3\gamma_4\|\boldsymbol{\eta}\|$ for some $\gamma_4 > 0$ independent of θ.

Furthermore, [10] also presents the LFC, $W(t, \tilde{r}, \tilde{s}, \tilde{b}) = V(\tilde{s}) + 2\,l\,\tilde{s}\,\tilde{r}^\mathsf{T}\boldsymbol{R}(\boldsymbol{q}_b^n)\tilde{b} + \frac{l}{2k_I}\tilde{b}^\mathsf{T}\tilde{b} > 0, \forall \tilde{r}, \tilde{b} \neq 0$. By following the steps of [10, Proof, Theorem 1] result in

$$\dot{W} \leq -\begin{bmatrix}\|\tilde{r}\| & \|\tilde{b}\|\end{bmatrix}^\mathsf{T}\begin{bmatrix} k_P\,a - l\,M^2 & \star \\ -\frac{1}{2}(1 + 2\,l\,M_\omega) & l\,\epsilon^2\end{bmatrix}\begin{bmatrix}\|\tilde{r}\| \\ \|\tilde{b}\|\end{bmatrix} \quad (26)$$

where $\star$ indicates symmetry, $a > 0$ and $M_\omega \geq \|\boldsymbol{\omega}_{b/n}^b\|$. l is given in [10]. Moreover, from [10] for some sufficiently large k_P, can it be shown that $\dot{W} \leq -\kappa\|\tilde{\boldsymbol{\chi}}\|^2 < 0$ for some $\kappa > 0$. With the relations above we get that $\dot{W}$ is less or equal than $-\kappa\|\tilde{\boldsymbol{\chi}}\|^2$ plus the terms related to μ_1, $\boldsymbol{\mu}_2$ and $\boldsymbol{\mu}_3$, yielding that

$$\dot{W} \leq -\kappa\|\tilde{\boldsymbol{\chi}}\|^2 - 2\tilde{s}\mu_1 + 2l\mu_1\tilde{r}^\mathsf{T}\boldsymbol{R}(\boldsymbol{q}_b^n)\tilde{b} + 2l\tilde{s}\boldsymbol{\mu}_2^\mathsf{T}\boldsymbol{R}(\boldsymbol{q}_b^n)\tilde{b}$$
$$+ 2l\tilde{s}\tilde{r}^\mathsf{T}\boldsymbol{R}(\boldsymbol{q}_b^n)\boldsymbol{\mu}_3 + \frac{l}{k_I}\tilde{b}^\mathsf{T}\boldsymbol{\mu}_3.$$

Furthermore, by taking in account the bounds on μ_1, $\boldsymbol{\mu}_2$ and $\boldsymbol{\mu}_3$, it follows that

$$\dot{W} \leq -\kappa\|\tilde{\boldsymbol{\chi}}\|^2 + 2\theta^3\gamma_2\|\tilde{r}\|\|\boldsymbol{\eta}\| + 2l\theta^3\gamma_2\|\tilde{b}\|\|\boldsymbol{\eta}\|$$
$$+ 2l\theta^3\gamma_3\|\tilde{b}\|\|\boldsymbol{\eta}\| + 2l\theta^3\gamma_4\|\tilde{r}\|\|\boldsymbol{\eta}\| + \frac{l}{k_I}\theta^3\gamma_4\|\tilde{b}\|\|\boldsymbol{\eta}\|$$
$$\leq -\kappa\|\tilde{\boldsymbol{\chi}}\|^2 + \gamma_5\theta^3\|\tilde{\boldsymbol{\chi}}\|\|\boldsymbol{\eta}\|$$

for an appropriate constant γ_5, independent of θ.

Now, defining the LFC $Y := U + \frac{1}{\theta^7}W$ on the form of $\beta_1(\|\boldsymbol{\eta}\|^2 + \|\tilde{\boldsymbol{\chi}}\|^2) \leq Y \leq \beta_2(\|\boldsymbol{\eta}\|^2 + \|\tilde{\boldsymbol{\chi}}\|^2)$ where $\beta_1, \beta_2 > 0$. Then, the derivative of Y along the trajectories satisfies

$$\dot{Y} \leq -\lambda_{\min}(\boldsymbol{Q})\lambda_{\min}(\boldsymbol{P}^{-1})^2\|\boldsymbol{\eta}\|^2 + \frac{2\gamma_1}{\theta^4}\|\boldsymbol{P}^{-1}\|\|\boldsymbol{\eta}\|\|\tilde{\boldsymbol{\chi}}\|$$
$$- \frac{1}{\theta^7}\kappa\|\tilde{\boldsymbol{\chi}}\|^2 + \gamma_5\frac{1}{\theta^4}\|\tilde{\boldsymbol{\chi}}\|\|\boldsymbol{\eta}\|,$$

yielding

$$\dot{Y} \leq -\begin{bmatrix}\|\boldsymbol{\eta}\| & \|\tilde{\boldsymbol{\chi}}\|\end{bmatrix}\begin{bmatrix}\lambda_{\min}(\boldsymbol{Q})\lambda_{\min}(\boldsymbol{P}^{-1})^2 & \star \\ -\frac{2\|\boldsymbol{P}^{-1}\|\gamma_1+\gamma_5}{2\theta^4} & \frac{\kappa}{\theta^7}\end{bmatrix}\begin{bmatrix}\|\boldsymbol{\eta}\| \\ \|\tilde{\boldsymbol{\chi}}\|\end{bmatrix},$$

where $\star$ indicates symmetry. Clearly the first-order principal minor, $\lambda_{\min}(\boldsymbol{Q})\lambda_{\min}(\boldsymbol{P}^{-1})^2 > 0$, is positive. The second-order principal minor,

$$\frac{1}{\theta^7}\lambda_{\min}(\boldsymbol{Q})\lambda_{\min}(\boldsymbol{P}^{-1})^2\kappa - \frac{1}{\theta^8}\frac{(2\|\boldsymbol{P}^{-1}\|\gamma_1 + \gamma_5)^2}{4}$$

is positive for $\theta > \frac{(2\|\boldsymbol{P}^{-1}\|\gamma_1+\gamma_5)^2}{4\,\lambda_{\min}(\boldsymbol{Q})\lambda_{\min}(\boldsymbol{P}^{-1})^2\,\kappa}$. Inherently $\dot{Y} \leq -\beta_3(\|\boldsymbol{\eta}\|^2 + \|\tilde{\boldsymbol{\chi}}\|^2)$ for some $\beta_3 > 0$. By invoking the comparison Lemma [17, Lemma 3.4] with the linear system $\dot{u} = -\beta_3 u$, and the corresponding solution $u(t) = u(0)e^{-\beta_3 t}$ yields $Y(t) \leq Y(0)e^{-\beta_3 t}$ for all $t \geq 0$. Consequently, the equilibrium point $[\boldsymbol{\eta}^\mathsf{T}, \tilde{\boldsymbol{\chi}}^\mathsf{T}]^\mathsf{T} = \boldsymbol{0}$ is USGES as defined in Loria and Panteley [18, Def. 2.7]. ∎

Remark 1: The stability result of Theorem 1 is achieved for a sufficiently large θ and k_P, respectively. By studying the proof one can calculate the explicit minimum values of θ and k_P. However, θ and $k_1(t), k_2(t) \geq k_P$ will probably be unnecessary large due to the conservative nature of the proof. Therefore, the choice of gains should be based on careful tuning such that unnecessary amplification of sensor noise is prevented. Moreover, high gains in discretized systems can result in numerical instability. Hence, the gains should be chosen with care.

IV. CASE STUDY

This section presents a case study with time-varying gains illustrating how such gain strategy can yield higher performance and a more robust sensor fusion when GNSS quality changes.

A. DP Vessel and INS Configuration

The GNSS aided INS was applied to a simulated supply vessel in DP operation with two-set points. The vessel was exposed to environmental disturbances. These were irrotational current with fixed speed and first-order wave loads utilizing the JONSWAP wave spectra, see Fossen [15, Ch. 8] for details. The total 6 degrees of freedom vessel motion data were obtain using the Marine System Simulator [19] at 100 Hz. From this IMU data was generated at the same frequency. The GNSS' position measurements were obtained at 5 Hz. Zero mean Gaussian noise was added to all measurements Finally, the three axis gyro biases were simulated using $\boldsymbol{b}_g^b = 10^{-3} \cdot [-55,\, 35,\, -40]^\mathsf{T}$ rad/s.

B. Implementation

There exist other alternatives to calculate $\hat{\boldsymbol{\sigma}}$ than stated in (8). First, in the implementation we utilized a saturated estimate of $\hat{\boldsymbol{f}}^n$, denoted $\text{sat}_{M_f}(\hat{\boldsymbol{f}}^n)$, in order to prevent any peaking effects from initial transients to propagate from Σ_2 to Σ_1. Then, the choice of measurement and reference vectors, in the calculation of $\hat{\boldsymbol{\sigma}}$, was made with inspiration from the Triad algorithm [20]. The first vector pair was chosen to be the normalized versions of $\boldsymbol{f}^b$ and $\text{sat}_{M_f}(\hat{\boldsymbol{f}}^n)$, respectively. The second vector pair was chosen to normalized versions of $\boldsymbol{S}(\boldsymbol{f}^b)\boldsymbol{c}^b$ and $\boldsymbol{S}(\text{sat}_{M_f}(\hat{\boldsymbol{f}}^n))\boldsymbol{c}^n$, respectively. The proof of Theorem 1 is still valid for a uniformly bounded and Lipschitz continuous $\hat{\boldsymbol{\sigma}}$ with respect to $\text{sat}_{M_f}(\hat{\boldsymbol{f}}^n)$.

The innovation signal $\tilde{p}_z'$ should be high-pass filtered to remove any slow varying terms related to the height. These can e.g. come from tidal components. This also gives a low-pass effect since integration and high-pass filtering yield,

$$h(s) = \frac{1}{s} \cdot \frac{T_h\,s}{T_h s + 1} = T_h \cdot \frac{1}{T_h s + 1}. \quad (27)$$

Then, the high-pass filtered innovation can be extracted as:

$$\tilde{p}'_{z,h} = -\frac{1}{T_h}x_f + \tilde{p}'_z, \qquad (28)$$

where x_f is the low-pass filtered innovation signal.

The numerical integration was carried out with RK4 and the corrector-predictor scheme presented in [15, Ch.11.3.4].

C. Tuning and Gain Structure

The gains of $\boldsymbol{\Sigma}_1$, on compact form $g_a = [k_1(t), k_2(t), k_I(t)]^\intercal$, were chosen as:

$$\dot{g}_a = -\frac{1}{T}g_a + \frac{1}{T}k_a, \begin{cases} k_a = [20, 20, 1]^\intercal & \text{if } t \le 100 \\ k_a = [0.55, 1, 0.01]^\intercal & \text{else.} \end{cases}$$

with $T = 25$ s to speed up convergence of the $\hat{\boldsymbol{q}}_b^n$ and $\hat{\boldsymbol{b}}_g^b$. This strategy was compared to simulation with fixed attitude gains given as $k_1 = 0.55$, $k_2 = 1$ and $k_I = 0.01$.

The nominal gain of $\boldsymbol{\Sigma}_2$, $\boldsymbol{K}_0$, is obtained by solving (12) with $\boldsymbol{A}$, $\boldsymbol{C}$, $\boldsymbol{Q}$ and the scalar τ as design parameters. $\vartheta(t)$ can be chosen to any value larger than $\tau > 0$. $\vartheta(t)$ was based on the reported horizontal RMS error from the GNSS receiver. However, in addition to be GNSS noise dependent is also a higher initial $\vartheta(t)$ reasonable to speed up the convergence of $\boldsymbol{\Sigma}_2$. The following structure was chosen for $\vartheta(t)$:

$$\vartheta(t) = \vartheta_0 + \vartheta_1 + \vartheta_2 \qquad (29)$$

where $\vartheta_0 = 0.5$ and $\vartheta_1 = b \cdot e^{-a \cdot e_f}$ with $a = 2$ and $b = 1.5$. e_f is obtained by filtering the horizontal RMS GNSS error, $e_{\text{rms},xy}$, with a first-order low-pass filter with time constant, $T = 125$ s. $e_{\text{rms},xy}$ can be computed as:

$$e_{\text{rms},xy} = \sqrt{\sigma_x^2 + \sigma_y^2} = \sigma_{\text{ure}} \cdot HDOP \qquad (30)$$

such as in [21, Eq. (2.27)] where σ_x and σ_y are the north and east GNSS standard deviation, respectively whereas HDOP is the horizontal dilution of precision. σ_{ure} is the standard deviation of the user equivalent range measurements. The signal ϑ_2 is calculated as

$$\dot{\vartheta}_2 = -\frac{1}{T}\vartheta_2 + \frac{1}{T}k, \begin{cases} k = 1 & \text{if } t \le 100 \\ k = 0 & \text{else} \end{cases} \qquad (31)$$

with $T = 25$ s and is used to prescribe a higher gain initially in order to obtain faster convergence. After some time ϑ_2 will vanish and $\vartheta(t)$ will only depend on ϑ_0 and ϑ_1. Such a strategy introduces additional degrees of freedom in the sense that the position, velocity and acceleration estimates will be less sensitive to high GNSS measurement noise. Other methods instead of (29)–(31) can also be used.

The parameters related to $\boldsymbol{K}_0$ were chosen as $\tau = 1/2$ and $\boldsymbol{Q} = \text{blkdiag}\{50, 0.5 \cdot \boldsymbol{I}_{3\times3}, 0.08 \cdot \boldsymbol{I}_{3\times3}, 0.0025 \cdot \boldsymbol{I}_{3\times3}\}$, yielding $K_{p'_z p'_z} = 5.4295$, $K_{pp'_z} = 2.2396$, $K_{vp'_z} = 0.4454$, $K_{\xi p'_z} = 0.0354$ and $\boldsymbol{K}_{pp} = 0.9513 \cdot \boldsymbol{I}_{2\times2}$, $\boldsymbol{K}_{vp} = 0.3275 \cdot \boldsymbol{I}_{2\times2}$, $\boldsymbol{K}_{\xi p} = 0.0354 \cdot \boldsymbol{I}_{2\times2}$, respectively. θ was chosen to $\theta = 1$. The time constant of the high-pass filter was chosen as to be $T_h = 600$ in order to compensate for the slowly varying effect of ocean tides.
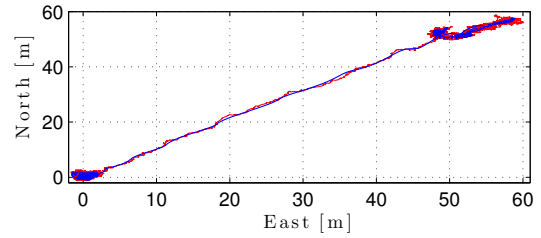

Fig. 2. Horizontal position of the DP vessel. Blue: True position. Red: Estimated position.
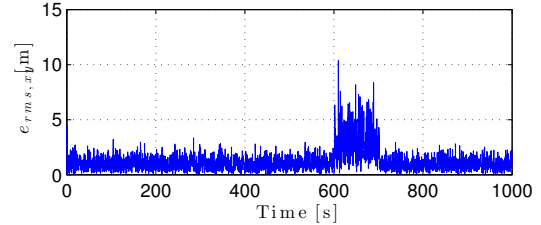

Fig. 3. Horizontal GNSS RMS accuracy.

D. Results

This section presents the simulation results. Fig. 2 shows the true horizontal position and estimates, respectively of the vessel during DP operation with two set-points. Furthermore, Fig. 3 shows how the reported horizontal GNSS RMS accuracy is reduced between time $t = 600$ s and $t = 700$ s. The resulting $\vartheta(t)$ is shown in Fig. 4 where one can observe the effects of the three gain components. For approximately $t < 150$ s is the dominating terms of (29), ϑ_0 and ϑ_2. ϑ_2 vanishes after $t > 150$ s. Furthermore, ϑ_0 is the main component of ϑ in the time interval $t = [600 - 700]$ s since ϑ_1 is the exponential decaying when GNSS accuracy is low.

The quality of heave estimates are shown in Fig. 5. It is seen that the heave estimates have a positive phase relative to the actual heave signal. This is to due to the high-pass filtering of the innovation signal $\tilde{p}'_z$. Reduction of the phase can be obtained with a different high-pass filter and by tuning of the filter time constant, T_h, as done in [16].

The estimation error of $\tilde{\boldsymbol{p}}$ with time-varying and fixed gains are presented in Figs 6 and 7, respectively. The RMS error of the position estimates, when GNSS quality was low with variable gains, resulted in $e_{\text{rms},\tilde{p}_x} = 0.6977$ and $e_{\text{rms},\tilde{p}_y} = 0.5751$, while the RMS errors were $e_{\text{rms},\tilde{p}_x} = 0.8158$ and $e_{\text{rms},\tilde{p}_y} = 0.8894$ with fixed gains.
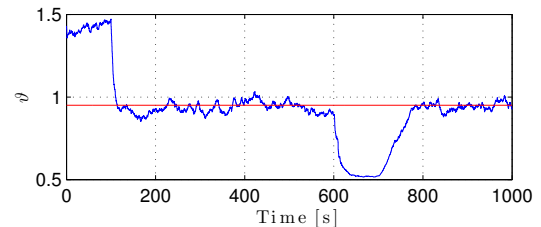

Fig. 4. The time-varying gain component, $\vartheta(t)$, in $\boldsymbol{\Sigma}_2$. Blue: Simulation with time-varying $\vartheta(t)$. Red: Simulation with fixed $\vartheta(t)$.
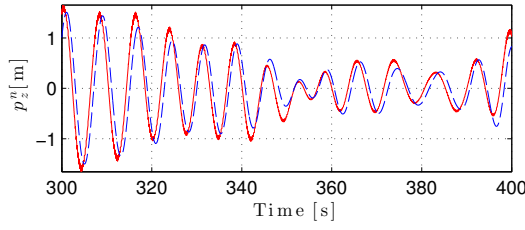
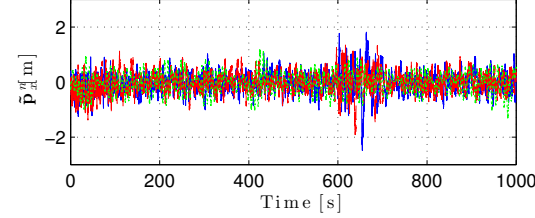Fig. 5. Illustration of the heave estimate quality. Blue: Heave of vessel. Red: Estimated heave.

Fig. 6. Position estimate error, $\tilde{\boldsymbol{p}}$ with time-varying gains. Blue: $\tilde{p}_x$. Red: $\tilde{p}_y$. Green: $\tilde{p}_z$.
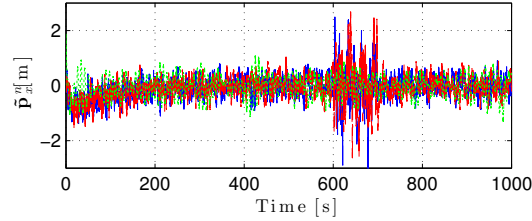

Fig. 7. Position estimate error, $\tilde{\boldsymbol{p}}$ with fixed gains. Blue: $\tilde{p}_x$. Red: $\tilde{p}_y$. Green: $\tilde{p}_z$.

Fig. 9. Attitude estimation error, given in Euler angles, with time-varying gains. Blue: Roll. Red: Pitch. Green: Yaw

Fig. 10. Attitude estimation error, given in Euler angles, with fixed gains. Blue: Roll. Red: Pitch. Green: Yaw

Fig. 11. Gyro bias estimation errors with time-varying gains. Blue: x-axis. Red: y-axis. Green: z-axis

The time evolution of the attitude gains can be seen in Fig. 8. Furthermore, in Figs. 9 and 10, the attitude estimation error are presented with time-varying and fixed gains, respectively. The convergence of the attitude estimates are observed to be significantly faster with time-varying gains. Such functionality is particular useful if a critical fault has occurred and the observers are re-initialized. By comparing Figs. 9 and 10 one can also observe less attitude error in roll and pitch with the time-varying gains when the GNSS quality was low. This is due to $\boldsymbol{\xi}$, in (9d)–(9e), was less affected by the GNSS noise in the time-varying case since $\vartheta(t)$ was reduced. Inherently, since $\hat{\boldsymbol{f}}^n$, in (9e), is utilized as reference vector in $\boldsymbol{\Sigma}_1$, the attitude will be less affected by GNSS noise. Finally, Fig. 11 show the decaying gyro bias estimation error when time-varying gains are utilized.
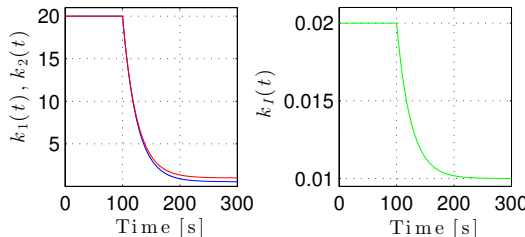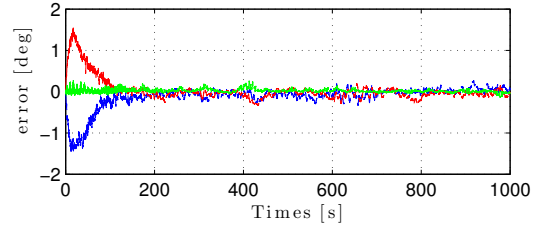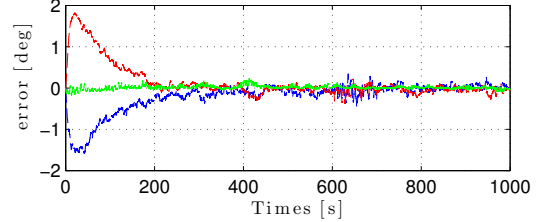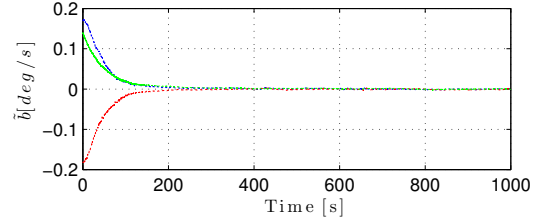
V. CONCLUSIONS

A uniformly semiglobal exponentially stable observer for GNSS aided INS tailored for DP vessels was developed. Time-varying gains were introduced to increase performance and robustness. Moreover, through simulations it was shown that time-varying gains in estimation of translational motion and attitude are beneficial for fast convergence and suppression of sensor noise.

APPENDIX I
STATE TRANSFORMATION

The estimation error of $\boldsymbol{\Sigma}_2$, $\tilde{\boldsymbol{x}} = [\tilde{p}'_z, \tilde{\boldsymbol{p}}, \tilde{\boldsymbol{v}}, \tilde{\boldsymbol{f}}]^\intercal$, can be transformed into the error variable $\boldsymbol{\eta}$ by defining: $\boldsymbol{\eta} := \boldsymbol{L}_\theta \tilde{\boldsymbol{x}}$ where $\boldsymbol{L}_\theta = \mathrm{blkdiag}\{1, \frac{1}{\theta}\boldsymbol{I}_{3\times3}, \frac{1}{\theta^2}\boldsymbol{I}_{3\times3}, \frac{1}{\theta^3}\boldsymbol{I}_{3\times3}\}$, θ is a high-gain like parameter. The error dynamics from (13) yield

$$\dot{\tilde{\boldsymbol{x}}} = (\boldsymbol{A} - \vartheta(t)\boldsymbol{K}_\theta\boldsymbol{C})\tilde{\boldsymbol{x}} + \boldsymbol{B}\tilde{\boldsymbol{d}}. \qquad (32)$$

with the $\boldsymbol{A}$, $\boldsymbol{B}$ and $\boldsymbol{C}$ matrices together with $\tilde{\boldsymbol{d}}$ and $\vartheta(t) \geq \tau$ from Section III-B–III-C. Let the total gain be calculated as

$$\vartheta(t)\boldsymbol{K}_\theta = \vartheta(t)\theta\boldsymbol{L}_\theta^{-1}\boldsymbol{K}_0. \qquad (33)$$

with $\boldsymbol{K}_0$ from Theorem 1. Moreover, by defining $\boldsymbol{\eta} := [\eta_1, \boldsymbol{\eta}_2, \boldsymbol{\eta}_3, \boldsymbol{\eta}_4]^\intercal$ with $\eta_1 := \tilde{p}'_z$, $\boldsymbol{\eta}_2 := \tilde{\boldsymbol{p}}/\theta$, $\boldsymbol{\eta}_3 := \tilde{\boldsymbol{v}}/\theta^2$ and $\boldsymbol{\eta}_4 := \tilde{\boldsymbol{f}}/\theta^3$, is the transformed error dynamics written

$$\dot{\boldsymbol{\eta}} = \dot{\boldsymbol{L}}_\theta \boldsymbol{x} + \boldsymbol{L}_\theta \dot{\boldsymbol{x}} = \boldsymbol{L}_\theta \dot{\boldsymbol{x}}. \qquad (34)$$

Fig. 8. Time-varying attitude gains. Blue: $k_1(t)$. Red: $k_2(t)$. Green: $k_I(t)$

It can also be shown that

$$\boldsymbol{L}_\theta(\boldsymbol{A}-\vartheta(t)\boldsymbol{K}_\theta\boldsymbol{C})\boldsymbol{L}_\theta^{-1} = \theta(\boldsymbol{A} - \vartheta(t)\boldsymbol{K}_0\boldsymbol{C}) \qquad (35)$$

and

$$\boldsymbol{L}_\theta\boldsymbol{B} = [0,\boldsymbol{0}_{3\times1}^\mathsf{T},\boldsymbol{0}_{3\times1}^\mathsf{T},1/\theta^3\cdot\boldsymbol{1}_{3\times1}^\mathsf{T}]^\mathsf{T} \qquad (36)$$

from

$$\dot{\boldsymbol{\eta}} = \boldsymbol{L}_\theta(\boldsymbol{A} - \vartheta(t)\boldsymbol{K}_\theta\boldsymbol{C})\boldsymbol{L}_\theta^{-1}\boldsymbol{\eta} + \boldsymbol{L}_\theta\boldsymbol{B}\tilde{\boldsymbol{d}} \qquad (37)$$

which again results in

$$\frac{1}{\theta}\dot{\boldsymbol{\eta}} = (\boldsymbol{A} - \vartheta(t)\boldsymbol{K}_0\boldsymbol{C})\boldsymbol{\eta} + \boldsymbol{\rho}(t,\tilde{\boldsymbol{\chi}}) \qquad (38)$$

with $\boldsymbol{\rho}(t,\tilde{\boldsymbol{\chi}}) = \frac{1}{\theta^4}[0,\boldsymbol{0}_{3\times1}^\mathsf{T},\boldsymbol{0}_{3\times1}^\mathsf{T},\tilde{\boldsymbol{d}}^\mathsf{T}]^\mathsf{T}$.

APPENDIX II
UNIFORM ATTRACTIVITY OF $\boldsymbol{\Sigma}_2$

Drawing upon the elements of [14, Lemma 2], is the origin of $\tilde{\boldsymbol{x}}$ proven to be uniformly attractive and stable.

Lemma 1 (Uniform Attractivity and Stability): For any $\delta > 0$ and $T > 0$ there exist a $\theta_1^* \geq 1$ such that for $\theta \geq \theta_1^*$ and all initial condition as specified in Theorem 1 results in $\|\tilde{\boldsymbol{x}}\| \leq \delta$ for all $t \geq T$. Hence, $\tilde{\boldsymbol{x}} = \boldsymbol{0}$ is an uniformly attractive and stable equilibrium point.

Proof: The proof follows as in [14, Proof Lemma 2]. The parameter projection in (7b) ensures $\|\tilde{\boldsymbol{b}}\| \leq M$ and because $\|\tilde{\boldsymbol{r}}\| \leq 1$, we have that $\|\tilde{\boldsymbol{\chi}}\| \leq \sqrt{M^2 + 1}$. Furthermore, we define the level set $\Omega_\theta := \{\boldsymbol{\eta} \,|\, U \leq \frac{\delta^2}{\theta^7}\lambda_{\min}(\boldsymbol{P}^{-1})\}$, and note that $\boldsymbol{\eta} \in \Omega_\theta \Rightarrow \|\boldsymbol{\eta}\| \leq \frac{\delta}{\theta^3} \Rightarrow \|\tilde{\boldsymbol{x}}\| \leq \delta$. Outside of Ω_θ, we have $\|\boldsymbol{\eta}\| \geq \frac{\delta}{\theta^3}\sqrt{\lambda_{\min}(\boldsymbol{P}^{-1})/\lambda_{\max}(\boldsymbol{P}^{-1})}$ which implies that $\dot{U}$ can be stated as

$$\dot{U} \leq -\frac{1}{2}\lambda_{\min}(\boldsymbol{Q})\lambda_{\min}(\boldsymbol{P}^{-1})^2\|\boldsymbol{\eta}\|^2$$
$$-\left(\frac{\delta\sqrt{\lambda_{\min}(\boldsymbol{P}^{-1})}\sqrt{\lambda_{\min}(\boldsymbol{Q})\lambda_{\min}(\boldsymbol{P}^{-1})^2}}{2\theta^3\sqrt{\lambda_{\max}(\boldsymbol{P}^{-1})}}\right.$$
$$\left.-\frac{2\|\boldsymbol{P}^{-1}\|\gamma_1}{\theta^4}\sqrt{M^2 + 1}\right)\|\boldsymbol{\eta}\|$$
$$= -\frac{1}{2}\lambda_{\min}(\boldsymbol{Q})\lambda_{\min}(\boldsymbol{P}^{-1})^2\|\boldsymbol{\eta}\|^2$$
$$-\left(\frac{\delta\sqrt{\lambda_{\min}(\boldsymbol{Q})}\lambda_{\min}(\boldsymbol{P}^{-1})^{\frac{3}{2}}}{2\theta^3\sqrt{\lambda_{\max}(\boldsymbol{P}^{-1})}} - \frac{2\|\boldsymbol{P}^{-1}\|\gamma_1}{\theta^4}\sqrt{M^2 + 1}\right)\|\boldsymbol{\eta}\|.$$

by utilizing (19). The first term is negative definite. The second term can be made negative definite with a sufficiently large θ, yielding

$$\dot{U} \leq -\frac{1}{2}\lambda_{\min}(\boldsymbol{Q})\lambda_{\min}(\boldsymbol{P}^{-1})^2\|\boldsymbol{\eta}\|^2$$
$$\leq -\frac{\theta}{2}\frac{\lambda_{\min}(\boldsymbol{Q})\lambda_{\min}(\boldsymbol{P}^{-1})^2}{\lambda_{\max}(\boldsymbol{P}^{-1})}U$$

outside Ω_θ. Defining a as:

$$a := \theta\,\lambda_{\min}(\boldsymbol{Q})\lambda_{\min}(\boldsymbol{P}^{-1})^2/(2\lambda_{\max}(\boldsymbol{P}^{-1}))$$

and invoking the comparison Lemma [17, Lemma 3.4] with $\dot{u} = -au$ and the corresponding solution $u(t) \leq u(0)e^{-at}$ we get: $U(t) \leq U(0)e^{-at}$. By letting $L > \delta$ be a bound on $\|\tilde{\boldsymbol{x}}(0)\|$ for any initial condition as specified in Theorem 1, then L is also a bound on $\|\boldsymbol{\eta}(0)\|$. Then, outside Ω_θ we have

$$U(t) \leq \frac{\lambda_{\max}(\boldsymbol{P}^{-1})L^2}{\theta}\exp\left(-\frac{\theta}{2}\frac{\lambda_{\min}(\boldsymbol{Q})\lambda_{\min}(\boldsymbol{P}^{-1})^2}{\lambda_{\max}(\boldsymbol{P}^{-1})}t\right).$$

Thus, $\boldsymbol{\eta}$ must enter Ω_θ before

$$t \leq T = \frac{2\lambda_{\max}(\boldsymbol{P}^{-1})}{\lambda_{\min}(\boldsymbol{Q})\lambda_{\min}(\boldsymbol{P}^{-1})^2\theta}\left[6\ln(\theta) + \ln\left(\frac{L^2\lambda_{\max}(\boldsymbol{P}^{-1})}{\delta^2\lambda_{\min}(\boldsymbol{P}^{-1})}\right)\right].$$

Hence, for a sufficiency large $\theta \geq 1$, $\|\tilde{\boldsymbol{x}}\| \leq \delta$ for $t \geq T$. ∎

REFERENCES

[1] P. Maybeck, "Stochastic models, estimation, and control, volume 1," in *Mathematics in Science and Engineering*. Academic Press, 1979, vol. 141.

[2] J. A. Farrell, *Aided Navigation: GPS with High Rate Sensors*. McGraw-Hill, 2008.

[3] S. Salcudean, "A globally convergent angular velocity observer for rigid body motion," *IEEE Trans. Automat. Contr.*, vol. 36, no. 12, pp. 1493 – 1497, 1991.

[4] J. Thienel and R. Sanner, "A coupled nonlinear spacecraft attitude controller and observer with an unknown constant gyro bias and gyro noise," *IEEE Trans. Automat. Contr.*, vol. 48, no. 11, pp. 2011–2014, 2003.

[5] B. Vik and T. Fossen, "A nonlinear observer for GPS and INS integration," in *Proc. IEEE Conf. Dec. Cont*, vol. 3, Orlando, FL, December 2001, pp. 2956–61.

[6] R. Mahony, T. Hamel, and J. M. Pflimlin, "Nonlinear complementary filters on the special orthogonal group," *IEEE Trans. Automat. Contr.*, vol. 53, no. 5, pp. 1203–2018, 2008.

[7] M.-D. Hua, "Attitude estimation for accelerated vehicles using GPS/INS measurements," *Control Engineering Practice*, vol. 18, no. 7, pp. 723–732, 2010.

[8] P. Batista, C. Silvestre, and P. Oliveira, "A GES attitude observer with single vector observations," *Automatica*, vol. 48, no. 2, pp. 388–39, 2012.

[9] ——, "Globally exponentially stable cascade observers for attitude estimation," *Control Engineering Practice*, vol. 20, no. 2, pp. 148–155, 2012.

[10] H. F. Grip, T. I. Fossen, T. A. Johansen, and A. Saberi, "Attitude estimation using biased gyro and vector measurements with time-varying reference vectors," *IEEE Trans. Automat. Contr.*, vol. 57, no. 5, pp. 1332—1338, 2012.

[11] A. Roberts and A. Tayebi, "On the attitude estimation of accelerating rigid-bodies using GPS and IMU measurements," in *Proc. Conf. Dec. Cont. and European Cont. Conf.*, Orlando, FL, December 2011, pp. 8088–8093.

[12] H. F. Grip, T. I. Fossen, T. A. Johansen, and A. Saberi, "A nonlinear observer for integration of gnss and imu measurements with gyro bias estimation," in *Proc. of the American Contr. Conf.*, Montreal, Canada, June 2012, pp. 4607–4612.

[13] H. F. Grip, A. Saberi, and T. A. Johansen, "Observers for interconnected nonlinear and linear systems," *Automatica*, vol. 48, no. 7, pp. 1339–1346, 2012.

[14] H. F. Grip, T. I. Fossen, T. A. Johansen, and A. Saberi, "Nonlinear observer for gnss-aided inertial navigation with quaternion-based attitude estimation," in *Proc. of the American Contr. Conf.*, Washington, DC, June 2013, pp. 272–279.

[15] T. I. Fossen, *Handbook of Marine Craft Hydrodynamics and Motion Control*. John Wiley & Sons, Ltd., 2011.

[16] J.-M. Godhavn, "Adaptive tuning of heave filter in motion sensor," in *OCEANS '98 Conf. Proc.*, Nice, France, 28 Sept.–1 Oct. 1998.

[17] H. K. Khalil, *Nonlinear Systems*, 3rd ed. Prentice Hall, 2002.

[18] A. Loria and E. Panteley, "Cascaded nonlinear time-varying systems: Analysis and design," in *Adv. Top. in Cntrl. Sys. Theory*, ser. LNCIS, F. Lamnabhi-Lagarrigue, A. Loria, and E. Panteley, Eds. Springer-Verlag, 2005, no. 311, ch. 2, pp. 23–64.

[19] "MSS. Marine Systems Simulator," www.marinecontrol.org, 2010.

[20] M. D. Shuster and S. D. Oh, "Three-axis attitude determination from vector observations," *Journal of Guidance Control and Dynamics*, vol. 4, no. 1, 1981.

[21] P. Misra and P. Enge, *Global Positioning System: Signals, Measurements, and Performance*, 2nd ed. Ganga-Jamuna Press, 2011.